Armenian Journal of Physics, 2010, vol. 3, issue 2, pp. 138-149

ANALYSIS OF DYNAMIC AND STATIC CHARACTERISTICS OF InGaAs/GaAs SELF-ASSEMBLED QUANTUM DOT LASERS

D. Ghodsi, H. Arabshahi and M. Rezaee Rokn-Abadi

Department of Physics, Faculty of Science, Ferdowsi University of Mashhad, Mashhad, Iran
E-mail: arabshahi@um.ac.ir

Received 08 November, 2009

Abstract: We have solved the rate equations for InGaAs/GaAs self-assembled quantum-dot laser considering homogeneous and inhomogeneous broadening of optical gain numerically using fourth-order Runge-Kutta method. Dynamic-characteristics are analyzed; relaxation oscillation frequency, modulation bandwidth, and turn-on delay improve as injection current increases. With enhancing of the full width at half maximum (FWHM) of homogeneous broadening, threshold current and turn-on delay increase, because of elevating of central group density of states. Simulation results of static-characteristics show that slope-efficiency increases as the FWHM of homogeneous broadening heightens due to enhancing of central group carriers. Exceeding of the FWHM of homogeneous broadening from FWHM of inhomogeneous broadening results in degradation of slope-efficiency and static-characteristics because empty DOS increas. Nonlinearity appears in light-current characteristics at a special interval from ratio of FWHM of homogeneous broadening to FWHM of inhomogeneous broadening. Differential gain decreases as initial relaxation time and recombination times heighten. Consequently, relaxation oscillation frequency and modulation bandwidth decline.

Keywords: Quantum-dot laser; optical gain; Runge–Kutta method; modulation bandwidth

1. Introduction

The emergence of devices based on nanometer-size active elements marked the era of nanoelectronics and nanophotonics. Among such elements are notably low-dimensional heterostructures, such as quantum wells (QWs), quantum wires (QWRs), and quantum dots (QDs). Quantum confinement in low-dimensional heterostructure strongly modifies the basic properties of a semiconductor crystal.

In QDs carriers are three-dimensionally confined and the modification of electronic properties is quite stronger than QWs and QWRs. In QDs, the energy levels are discrete and transitions between electrons and holes are comparable with transitions between discrete levels of single atoms. Thus, QDs are also referred to as superatoms or artificial atoms [1].

Semiconductor laser is the fundamental device of modern optoelectronics and photonics. Due to unique three dimensional quantum confinement, QD lasers have demonstrated both theoretically and experimentally many superior properties, such as ultra-low and temperature-stable threshold current density, high optical gain, high-speed operation, broad modulation bandwidth, and narrow spectrum linewidth primarily due to the delta-function like density of states [2, 3]. However, we know that actual self-assembled QDs do not always meet our expectation because of the inhomogeneous and homogeneous broadening of the optical gain, phonon bottleneck. Thus, for an accurate and rigorous analysis of QD-LDs we need to take into account all these actual aspects of QDs [4].

In this paper, first, we describe QD laser analyzing theory based on the rate equations model and consider the homogeneous and inhomogeneous broadening of the optical gain for solving InGaAs/GaAs self-assembled quantum dot laser (SAQD-LD) rate equations numerically using fourth-order Runge–Kutta method. Then, in the result section, we achieve dynamic response and analyze carrier and photon time evolution of mentioned QD laser at different injected currents and FWHM of homogeneous broadening; also, we simulate static response and analyze the effects of inhomogeneous and homogeneous broadening on static-characteristics. Finally, the effects of recombination times and initial relaxation oscillation time are treated on optical gain-current-characteristics.

2. Optical Gain Theory

Based on the density-matrix theory, the linear optical gain of QD active region is given as

$$g^{(1)}(E) = \frac{2pe^2hN_D}{cn_re_0m_0^2}.\frac{\left|p_{cv}^s\right|^2(f_c - f_v)}{E_{cv}}B_{cv}(E - E_{cv}), \tag{1}$$

where n_r is the refractive index, N_D is the volume density of QDs, $\left|p_{cv}^s\right|$ is the transition matrix element, f_c is the electron occupation function of the conduction-band discrete state, f_v is that of the valence-band discrete state, and E_{cv} is the interband transition energy. The linear optical gain shows the homogeneous broadening of a Lorentz shape as

$$B_{cv}(E - E_{cv}) = \frac{hG_{cv}/p}{(E - E_{cv})^2 + (hG_{cv})^2}, \tag{2}$$

where FWHM is given as $2\hbar\Gamma_{cv}$ with polarization dephasing or scattering rate Γ_{cv}. Neglecting the optical-field polarization dependence, the transition matrix element is given as

$$\left|P_{cv}^s\right|^2 = \left|I_{cv}\right|^2 M^2, \tag{3}$$

where I_{cv} represents the overlap integral between the envelope functions of an electron and a hole, and

$$M^2 = \frac{m_0^2}{12m_e^*}\frac{E_g(E_g + D)}{E_g + 2D/3} \tag{4}$$

as derived by the first-order **kp** interaction between the conduction band and valence band. Here, E_g is the band gap, m_e^* is the electron effective mass, Δ is the spin-orbit interaction energy of the QD material. Equation (3) holds as long as we consider QDs with a nearly symmetrical shape

In actual SAQD-LDs, we should rewrite the linear optical gain formula of Eq. (1) by taking into account inhomogeneous broadening due to the QD size and composition fluctuation in terms of a convolution integral as

$$g^{(1)}(E) = \frac{2pe^2hN_D}{cn_r e_0^2} \cdot \frac{\left|p_{cv}^s\right|^2}{E_{cv}} (f_c(E) - f_v(E)).$$
$$B_{cv}(E - E_c)G(E_c - E_{cv})dE_c, \tag{5}$$

where E_{cv} is the center of the energy distribution function of each interband transition, $f_c(E_c)$is the electron occupation function of the conduction-band discrete state of the QDs with the interband transition energy of E_c, and $f_v(E_v)$ is that of the valence band discrete state. The energy fluctuation of QDs are represented by $G(E_c–E_{cv})$ that takes a Gaussian distribution function as

$$G(E_c - E_{cv}) = \frac{1}{\sqrt{2p}x_0} \exp(E_c - E_{cv})^2 / 2x_0^2, \tag{6}$$

whose FWHM is given by $\Gamma_0 = 2.35\xi_0$. The width Γ_0 usually depends on the band index *c* and ν [5].

3. Rate Equations

The most popular and useful way to deal with carrier and photon dynamics in lasers is to solve rate equations for carrier and photons. Fig. 1 illustrates the energy diagram of the conduction band of the self-assembled quantum dot laser active region, and diffusion, relaxation, recombination, and escape processes of carriers [5, 6]. We consider an electron and a hole as an exciton, thus, the relaxation means the process that both an electron and a hole relax into the ground state simultaneously to form an exciton. We assume that only a single discrete electron and hole ground state is formed inside the QD, and the charge neutrality always holds in each QD.

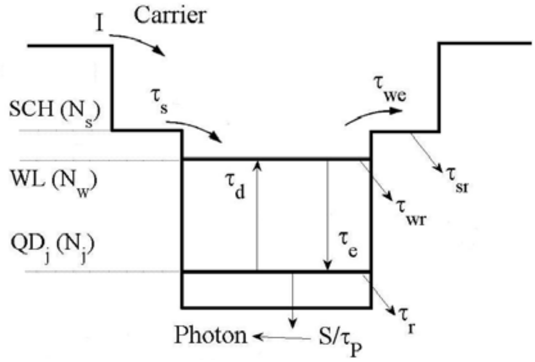

Fig. 1. Energy diagram of the laser-active region and diffusion, recombination, and relaxation processes.

In order to describe the interaction between the QDs with different resonant energies through photons, we divide the QD ensemble into j = 1, 2,... 2M+1 groups, depending on their resonant energy for the interband transition, over the longitudinal cavity photon modes. $j = M$ corresponds to the group and mode at E_{cv}. We take the energy width of each group equal to the mode separation of the longitudinal cavity photon modes which equals to

$$D_E = ch / 2n_r L_{ca}, \tag{7}$$

where L_{ca} is the cavity length. The energy of the *j*-th QDs group is represented by

$$E_j = E_{cv} - (M - j)D_E, \tag{8}$$

where $j = 1, 2, ..., 2\mathrm{M} + 1$. The QD density of *j*-th QDs group is given as

$$N_D G_j = N_D G(E_j - E_{cv})D_E. \tag{9}$$

Let N_j be the carrier number in *j*-th QDs group. According to Pauli's exclusion principle, the occupation probability in the ground state of the *j*-th QDs group is defined as

$$P_j = N_j / 2N_D V_a G_j. \tag{10}$$

The rate equations are as follows [4-8]

$$\frac{dN_s}{dt} = \frac{I}{e} - \frac{N_s}{\tau_s} - \frac{N_s}{\tau_{sr}} + \frac{N_w}{\tau_{we}}, \tag{11}$$

$$\frac{dN_w}{dt} = \frac{N_s}{\tau_s} + \frac{N_j}{\tau_e D_g} - \frac{N_w}{\tau_{wr}} - \frac{N_w}{\tau_{we}} - \frac{N_w}{\tau_d}, \tag{12}$$

$$\frac{dN_j}{dt} = \frac{N_w G_j}{\tau_{dj}} - \frac{N_j}{\tau_r} - \frac{N_j}{\tau_e D_j} - \frac{c\Gamma}{n_r} g^{(1)}(E) S_m, \tag{13}$$

$$\frac{dS_m}{dt} = \frac{\beta N_j}{\tau_r} + \frac{c\Gamma}{n_r} g^{(1)}(E) S_m - S_m / \tau_p, \tag{14}$$

where N_s, N_w, and N_j are the carrier number in separate confinement heterostructure (SCH) layer, wetting layer (WL) and *j*-th QDs group, respectively, S_m is the photon number of *m*-th mode, where *m* = 1,2…2M+1, *I* is the injected current, G_j is the fraction of the *j*-th QDs group type within an ensemble of different dot size populations, e is the electron charge, D_g is the degeneracy of the QD ground state without spin, β is the spontaneous-emission coupling efficiency to the lasing mode. $g_{mj}^{(1)}$ is the linear optical gain which the *j*-th QDs group gives to the *m*-th mode photons and is represented by

$$g_{mj}^{(1)}(E) = \frac{2\pi e^2 h N_D}{c n_r \varepsilon_0 e_0^2} \cdot \frac{\left|p_{cv}^s\right|^2}{E_{cv}} (2p_j - 1). \\ G_j B_{cv}(E_m - E_j). \tag{15}$$

The related time constants are, τ_s, diffusion in the SCH region, τ_{sr}, carrier recombination in the SCH region, τ_{we}, carrier reexcitation from the WL to the SCH region, τ_{wr}, carrier recombination in the WL, τ_{dj}, carrier relaxation into the *j*-th QDs group, τ_r, carrier recombination in the QDs, τ_p, photon lifetime in the cavity, The average carrier relaxation lifetime, $\overline{\tau}_d$, is given as

$$\tau_d^{-1} = \tau_{dh}^{-1}.G_n = \tau_d^{-1}(1-P_n)G_n, \tag{16}$$

where τ_o is the initial carrier relaxation lifetime. The photon lifetime in the cavity is

$$\tau_p^{-1} = c / n_r + \ln(1/R_1R_2)/2L_{cav}, \tag{17}$$

where R_1 and R_2 are the cavity mirror reflectivities, and α_i is the internal loss. The laser output power of the *m*-th mode from one cavity mirror is given a

$$I_m = hw_m cS_m \ln(1/R)/2L_{cav}n_r, \tag{18}$$

where ω_m is the emitted photon frequency, and R is R_1 or R_2.

We solved the rate equations numerically using fourth-order Runge-Kutta method to obtain the carrier and photon-characteristics, and modulation response by supplying the steplike current at time $t = 0$. The system reaches the steady-state after the relaxation oscillation. We assume that all the carriers are injected into the WL, i.e., $\tau_{sr} = \tau_{we} = \infty$, and consider the thermal carrier escape time $\tau_e = \infty$. It is assumed that QDs have a cylindrical shape. The parameters that we used at simulation are listed in Table 1 [5].

Table 1. Parameters used for simulation of InGaAs/GaAs SAQD-LD [5].

Parameter	**Sign**	**Value**
Radius of QD	R	8 nm
Height of QD	h	8 nm
Interband transition energy	E_{cv}	1 eV
Volume of QD	V_D	$\pi R^2 H$
Coverage of QDs	ξ	20%
Number of QD layer	N_W	3
Optical confinement factor	Γ_0	4%
Mirror reflectivities	R_1, R_2	30%, 90%
Internal loss	α	6 cm^{-1}
Stripe width	d	10 μm
Photon cavity lifetime	τ_P	8.8 ps
Cavity length	L	900 μm
FWHM of inhomogeneous broadening	Γ_0	20 meV
Initial carrier relaxation lifetime	τ_0	10 ps
Spin-orbit interaction energy	Δ	0.35 eV
Electron effective mass	m_e	$0.04m_0$
Spontaneous-emission coupling efficiency	β	10^{-4}
Refractive index	n_r	3.5
Band gap of bulk semiconductor	E_g	0.8 eV
Diffusion lifetime in the SCH region	τ_s	15 ps

4. Simulation Results

We have solved the rate equations (11) to (14) using numeric method of Runge-Kutta. Fig. 2 shows the simulation results of carrier-characteristics for different injection currents I=1.5, 2, 2.5, 5, and 10 mA at the FWHM of homogeneous broadenings (a) $\hbar\gamma_{cv} = 0.1$ meV and (b) $\hbar\gamma_{cv} = 10$ meV.

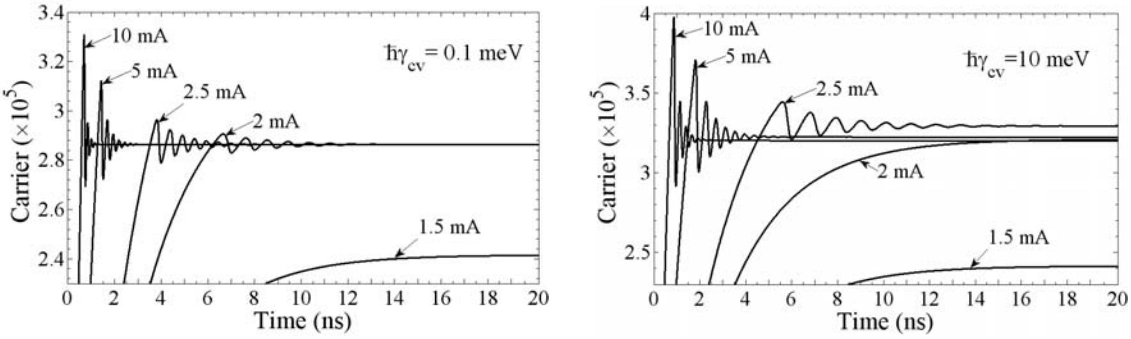

Fig. 2. Simulation results of carrier-characteristics for different injection currents *I* = 1.5, 2, 2.5, 5, and 10 mA at the FWHM of homogeneous broadenings: (a) $\hbar\gamma_{cv} = 0.1$ meV and (b) 10 meV.

As shown in Fig. 2, with increasing the injection current, turn on delay decreases, maximum of the relaxation oscillation magnitude and relaxation oscillation frequency enhance. Maximum of the relaxation oscillation magnitude increases and relaxation oscillation frequency degrades for the larger FWHM of homogeneous broadening.

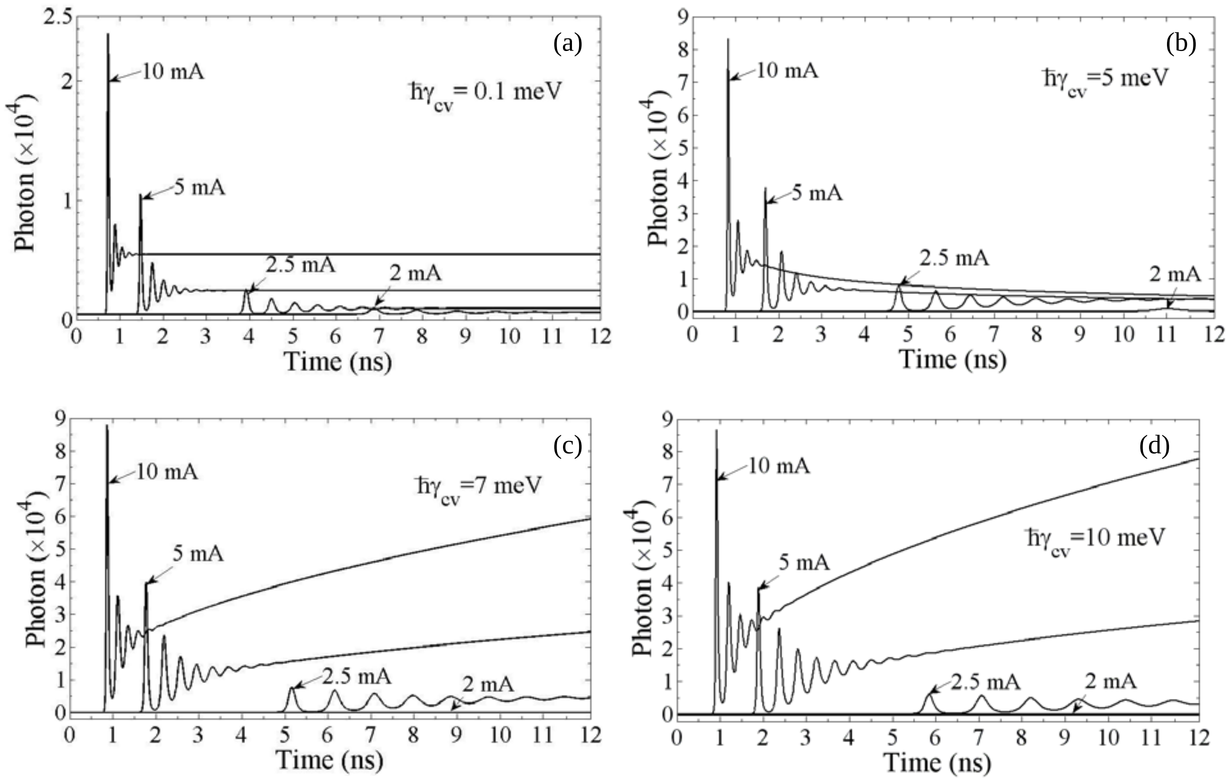

Fig. 3. Simulation results of photon characteristics for different injection currents *I* = 2, 2.5, 5, and 10 mA when the FWHM of homogeneous broadening is (a) $\hbar\gamma_{cv} = 0.1$ meV, (b) 5 meV, (c) 7 meV, and (d) 10 meV.

Fig. 3 shows the simulation results of photon-characteristics for different injection currents I=2, 2.5, 5, and 10 mA when the FWHM of homogeneous broadening is (a) $\hbar\gamma_{cv} = 0.1$ meV, (b) 5 meV, (c) 7 meV, and (d) 10 meV.

As shown in Fig. 3, the steady-state photons (output power) elevate as the injection current increases, except for Fig. 3(b) at the injection currents I = 5 and 10 mA. This is because, with increasing of the injection current, early, the carriers of QDs increase that result in enhancing of the cavity lasing photons, these increased photons that we call them early photons lead to elevating the stimulated emission rate, as a result the QDs carriers decrease (Fig. 2) and the lasing photons heighten at the new steady-state.

With increasing of the injection current, turn on delay degrades, this occurs because required carriers for start of the relaxation oscillation supply earlier. Relaxation oscillation frequency and maximum of the relaxation oscillation magnitude also enhance further increment of early photons leading to further increment of maximum of the relaxation oscillation magnitude. On the other hand, increasing of the stimulated emission rate leads to the rather light amplification and decreasing of the cavity photons time, consequently the relaxation oscillation frequency increases, and the laser reaches the steady-state earlier.

As the FWHM of homogeneous broadening heightens from (a) to (d), turn on delay increases, because DOS of the central group enhance, therefore the required carriers for beginning of lasing increase and are supply subsequent. Steady-state photons, except to Fig. 3(b) at the currents I = 5 and 10 mA, increase due to elevating of the QDs within the homogeneous broadening of the central mode, while emitting of the central group carriers within the other modes at the currents I = 5 and 10 mA (Fig. 3(b)) result in decreasing of the central mode steady-state photons. With increasing of the homogeneous broadening from 3 meV, the threshold current increases, because the steady-state photons at 2 mA decrease until at $\hbar\gamma_{cv} = 7$ meV the lasing emission becomes very weak and finally at $\hbar\gamma_{cv} = 10$ meV vanishes. Fig. 4 shows the photon-characteristics for I = 2 mA at (a) $\hbar\gamma_{cv} = 0.1$, 1, 3, 5 and 7 meV and (b) $\hbar\gamma_{cv} = 0.1$, 7.5, 8.5 and 10 meV.

Enhancing of the homogeneous broadening until special value for the specific current (for example, in Fig. 4(a), until $\hbar\gamma_{cv} = 3$ meV for I = 2 mA) leads to increasing of maximum of the relaxation oscillation magnitude and the steady-state photons, because the central group DOS and thus the central group carriers enhance. Further elevating of the homogeneous broadening results in heightening of the empty DOS at the central group (decreasing of the population inversion) and slaking of maximum of the relaxation oscillation magnitude and the steady-state photons. As shown at injection current I = 2 mA with increasing of the FWHM of homogeneous broadening from 6 meV, the population inversion is provided at the higher current and the threshold current elevates.

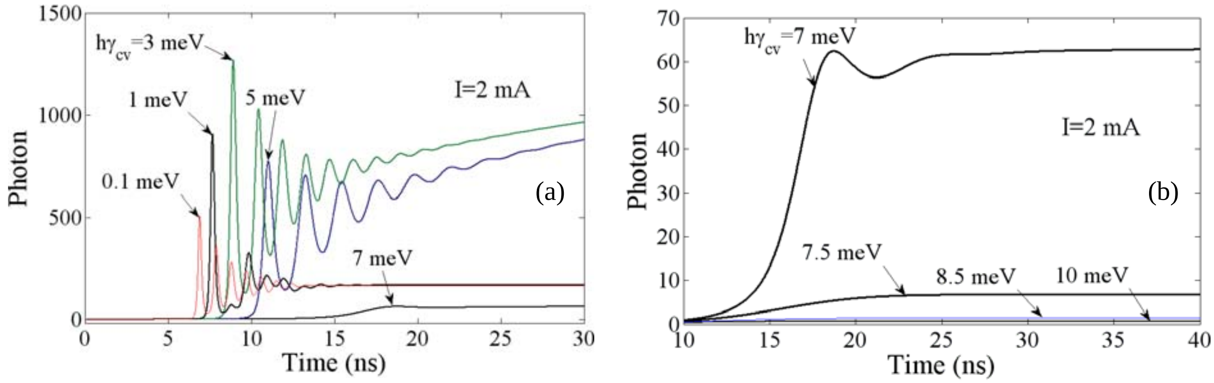

Fig. 4. Photon-characteristics for I = 2 mA at (a) $\hbar\gamma_{cv} = 0.1,\ 1,\ 3,\ 5$, and 7 meV, and (b) $\hbar\gamma_{cv} = 7,\ 7.5,\ 8.5$, 10 meV.

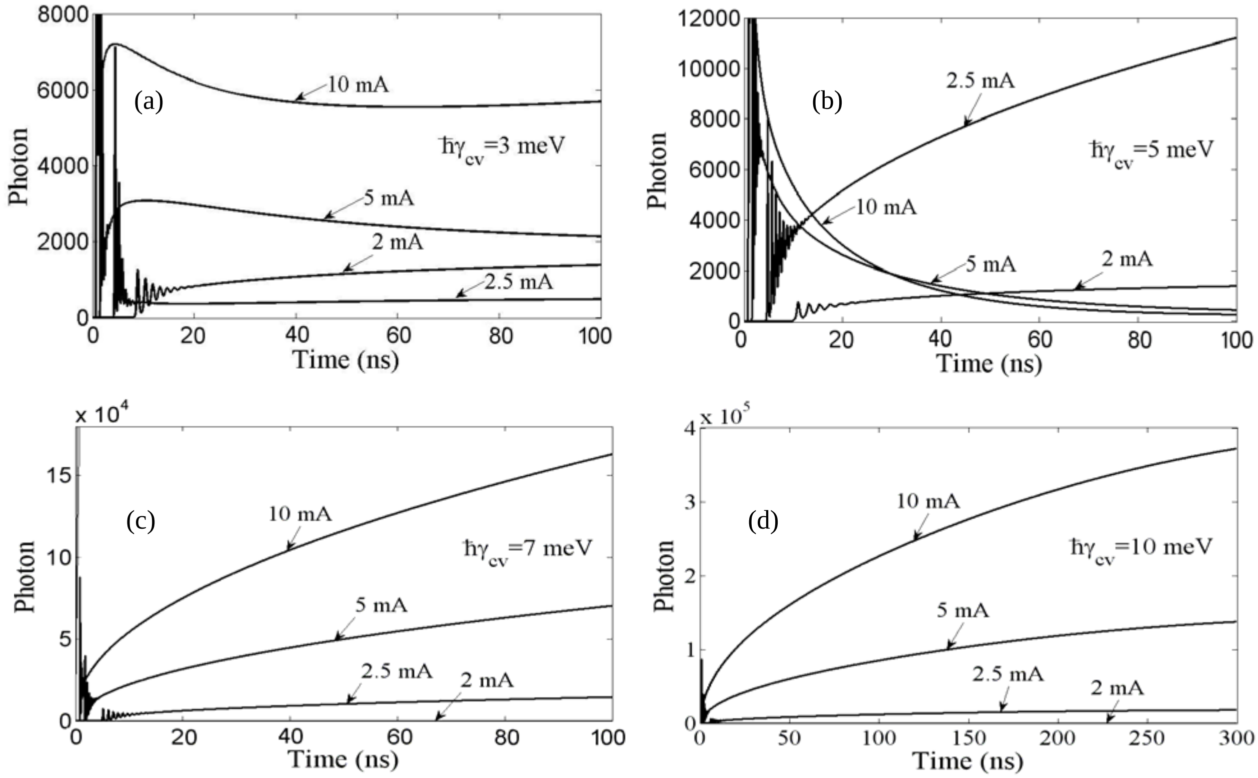

Fig. 5. Other illustration from photon characteristics for different injection currents I = 2, 2.5, 5, and 10 mA at (a) $\hbar\gamma_{cv} = 3$ meV (b) 5 meV, (c) 7 meV, (d) 10 meV.

Fig. 5 shows other illustration from photon-characteristics for different injection currents I = 2, 2.5, 5, and 10 mA at (a) $\hbar\gamma_{cv} = 3$ meV (b) 5 meV, (c) 7 meV, and (d) 10 meV.

As shown in Fig. 5(a), the steady-state photons at I = 2.5 mA are lesser than I = 2 mA. Lasing photons at I = 5 and 10 mA do not reach the steady state after 80 ns and 40 ns. As it is shown in Fig. 5(b), the lasing photons at I = 5 and 10 mA decrease as the time increases, and they become lesser than that of I = 2 mA after 45ns, they do not reach the steady-state after 80 ns. Lasing photons at 10 mA become lesser than that of 5 mA after 30ns. Lasing photons at I = 2.5 mA increase as the time enhances, and they do not reach the steady-state after 100ns. As it is shown in Fig. 5(c), the lasing photons at I = 2.5 mA reach the steady-state after 80ns, but, the lasing photons at I = 5 and 10 mA do not reach the steady-state and they elevate as the time increases. As it is shown in Fig. 5(d), the lasing photons at I = 5 and 10 mA do not reach the steady-state after 300ns. These non-steady-states are due to not considering of gain saturation effect.

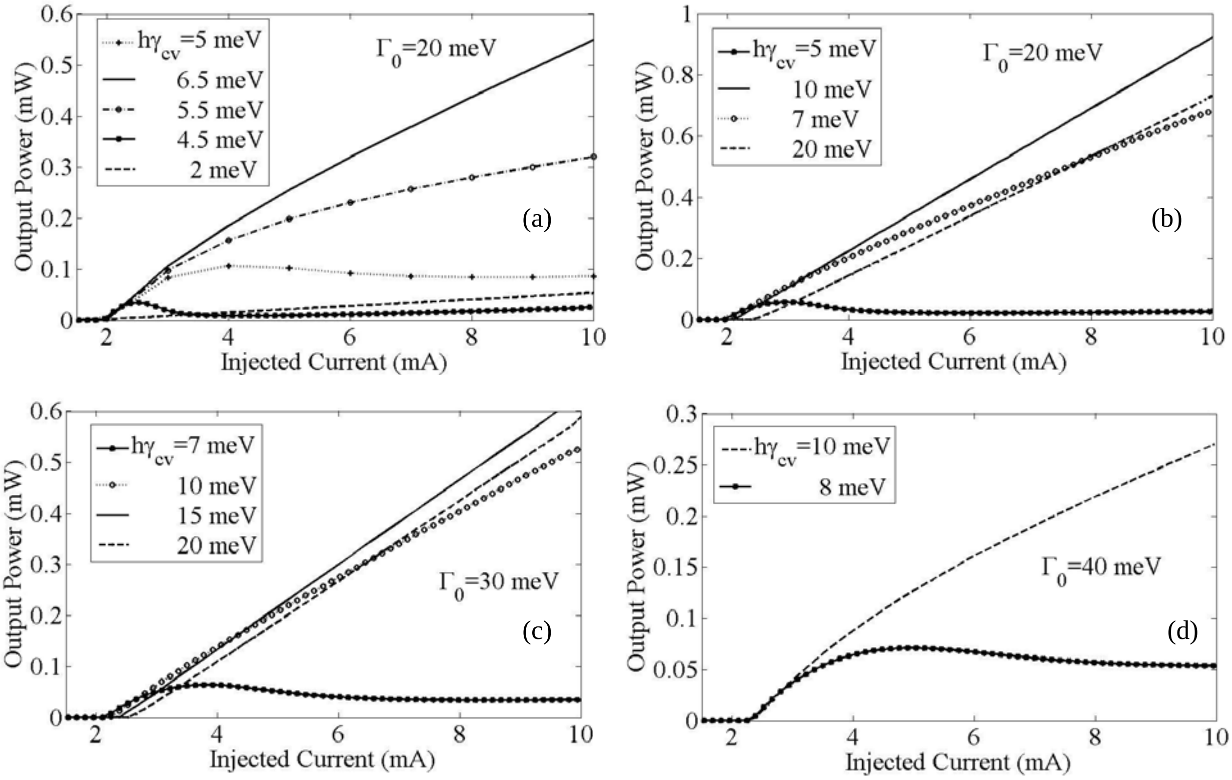

Fig. 6. Light-current characteristics of SAQD-LD for FWHM of inhomogeneous broadening Γ_0 = 20 meV at (a) $\hbar\gamma_{cv} = 2,\ 4.5,\ 5,\ 5.5$, and 6.5 meV and (b) $\hbar\gamma_{cv} = 5,\ 7$, 10, 15, and 20 meV and also FWHM of inhomogeneous broadenings (c) Γ_0 = 30 meV at $\hbar\gamma_{cv} = 7,\ 10$, 15, and 20 meV and (d) Γ_0 = 40 meV at $\hbar\gamma_{cv} = 8$ and 10 meV.

Fig. 6 shows light-current characteristics of SAQD-LD for FWHM of inhomogeneous broadening $\Gamma_0 = 20$ meV at different (a) $\hbar\gamma_{cv} = 2,\ 4.5$, 5, 5.5 and 6.5 meV and (b) $\hbar\gamma_{cv} = 5,\ 7$, 10 and 20 meV also FWHM of inhomogeneous broadenings (c) $\Gamma_0 = 30$ meV at $\hbar\gamma_{cv} = 7,\ 10$, 15 and 20 meV and (d) $\Gamma_0 = 40$ meV at $\hbar\gamma_{cv} = 7$ and 10 meV.

As we can see from Fig. 6(a) and 6(b), with increasing of FWHM of homogeneous broadening, non- linearity appears at L-I characteristics and continue to FWHM of homogeneous broadening become near to FWHM of inhomogeneous broadening. Slope efficiency (external quantum differential efficiency) heightens as the FWHM of homogeneous broadening increases from 10 meV where the FWHM of homogeneous broadening is half of the FWHM of inhomogeneous broadening, as a resulting of heightening of the central group carriers. Exceeding of the FWHM of homogeneous broadening from FWHM of inhomogeneous broadening results in degradation of slope efficiency due to increasing of the empty DOS. Threshold current increases as we see in Fig. 4. Fig. 6(c) and 6(d) show that slope efficiency decreases and threshold current also elevates with increasing of FWHM of inhomogeneous broadening as a resulting of decreasing of the central group DOS. Nonlinearity appears to further values of FWHM of homogeneous broadening in comparison of Fig. 6(d) to Fig. 6(b). We can infer that nonlinearity appears in a special interval from ratio of FWHM of homogeneous broadening to FWHM of inhomogeneous broadening. In some cases such as Fig. 6(a) at the FWHM of homogeneous broadening 9 meV and the certain current, all of the central group DOS occupy and the output power reaches a maximum and then it decrease as the injection current increases.

We can also see that enhancing of homogeneous broadening from inhomogeneous broadening leads to decline of static-characteristics of SAQD-LD.

Fig. 7 shows optical gain-current characteristics of SAQD-LD for different initial relaxation times $\tau_0 = 1$, 10, 100, 300 and 500 ps at different recombination times (a) $\tau_r = 2.8$ ns, $\tau_{qr} = 3$ ns, (b) $\tau_r = 2.8$ ns, $\tau_{qr} = 0.5$ ns, and (c) $\tau_r = 0.5$ ns, $\tau_{qr} = 0.5$ ns.

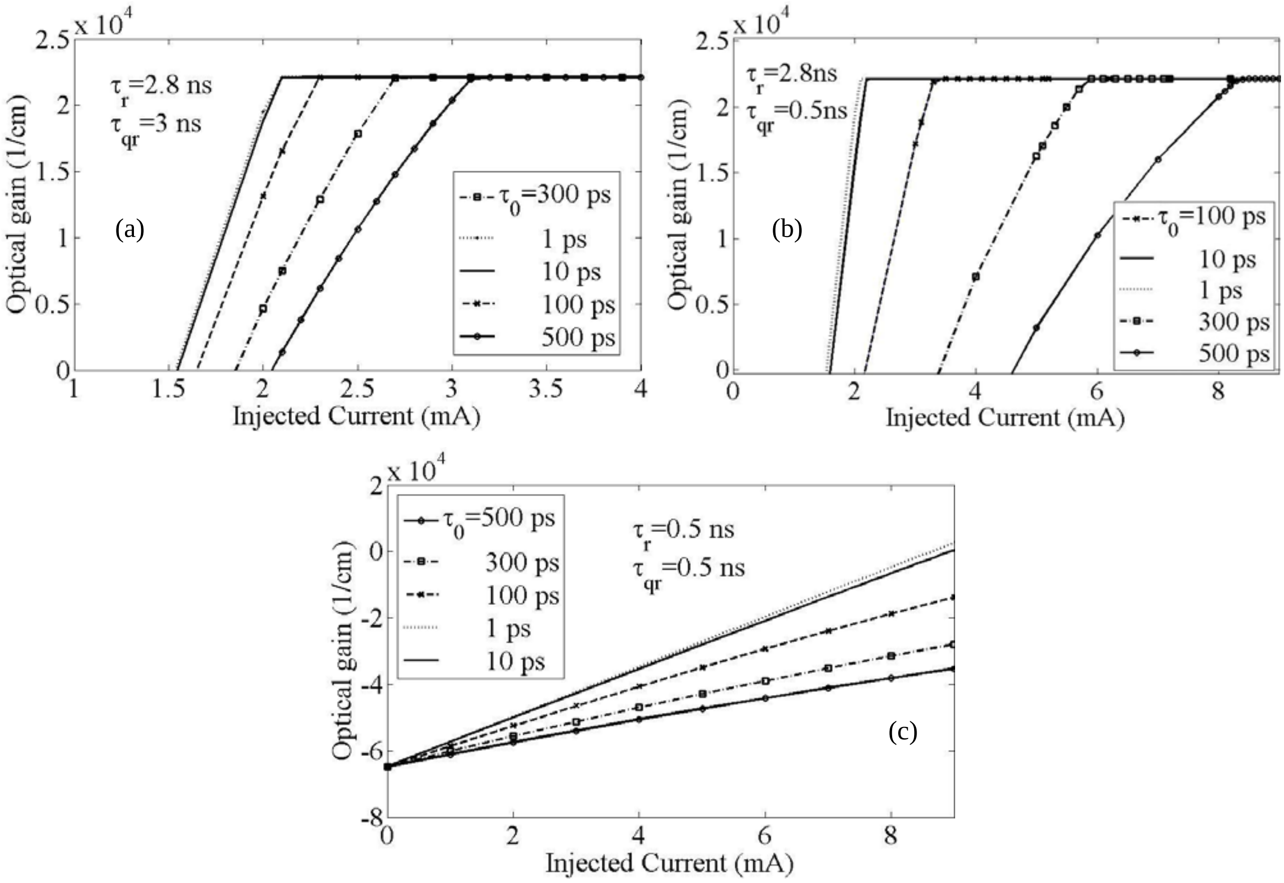

Fig. 7. Optical gain-current-characteristics of SAQD-LD for different initial relaxation times τ_0 = 1, 10, 100, 300, and 500 ps, at different recombination times: (a) τ_r = 2.8 ns, τ_{qr} = 3 ns, (b) τ_r = 2.8 ns, τ_{qr} = 0.5 ns, and (c) τ_r = 0.5 ns, τ_{qr} = 0.5 ns.

It seems that optical gain increases to the threshold gain and then becomes fixedness with enhancing of the injection current. Actually, what happens when the current is increased to a value above threshold is that the carrier density and gain initially (by the order of a nanosecond) elevate to values above their threshold levels, and the photon density grows. But then, the stimulated emission rate also heightens that leads to reducing of the carrier density and gain until a new steady-state balance is created [9]. Differential gain declines as the initial relaxation time and recombination times increase. Since the relaxation oscillation frequency has square direct relation with differential gain [10], the relaxation oscillation frequency and the modulation bandwidth decrease as the initial relaxation time and recombination time enhance. Fig. 7(c) shows that light amplification is linear beneath the lasing threshold.

5. Conclusion

Considering the homogeneous and inhomogeneous broadening of the optical gain, we solved the rate equations numerically using fourth-order Runge-Kutta method and analyzed the dynamic and static- characteristics of InGaAs/GaAs SAQD-LD. Dynamic characteristics and steady-state photons improve as the current increases. Threshold current and turn-on delay elevate, and maximum of the relaxation oscillation magnitude also enhances until special value and then decreases corresponding to the injection current as the FWHM of homogeneous broadening increases. Simulation results of the static-characteristics of InGaAs/GaAs SAQD-LD show that slope efficiency heightens as the FWHM of homogeneous broadening increases from where the FWHM of homogeneous broadening is half of the FWHM of inhomogeneous broadening. Exceeding of the FWHM of homogeneous broadening from FWHM of inhomogeneous broadening and elevating of the FWHM of inhomogeneous broadening result in degradation of slope efficiency. Threshold current increases as the homogeneous broadening and inhomogeneous broadening enhance. Nonlinearity appears in light-current-characteristics at a special interval from ratio of FWHM of homogeneous broadening to FWHM of inhomogeneous broadening. We also infer increasing of homogeneous broadening from inhomogeneous broadening leads to declining of static-characteristics of InGaAs/GaAs SAQD-LD. Optical gain increases to the threshold gain and then becomes fixedness with elevating of the injection current. Differential gain also decreases as the initial relaxation time and recombination times increase. Consequently, the relaxation oscillation frequency and the modulation bandwidth degrade.

ACKNOWLEDGMENT

We would like to thank Mrs Maryam Ghovani for her useful comments and writing up the paper.

References

1 **T. Steiner.** Semiconductor nanostructures for optoelectronic applications, Artech House, 2004.

2 **D. Bimberg**. Quantum Dot Heterostructures, John Wiley & Sons Inc, 1999.

3 **M. Sugawara.** Part of the SPIE Conference on Physics and Simulation of optoelectronic devises VI, v. 3283, 88 (1998).

4 **M. Sugawara.** J. Appl. Phys., v. 97, 043523 (2005).

5 **M. Sugawara**. Phys. Rev. B, v. 61, 7595 (2000).

6 **M. Sugawara.** Applied. Phys. Lett., v. 71, 2791 (1997).

7 **C. L. Tan.** Comput. Mater. Sci., 2008, doi: 10.1016/*j. commatsci*, 2008, 01.049.

8 **C. L. Tan, Y. Wang.** Applied Phys. Lett., v. 91, 061117 (2007).

9 **L. A. Coldren.** Diode Lasers and Photonic Integrated Circuits, John Wiley & Sons Inc, 1995.

10 **M. Sugawara.** Self -Assembled InGaAs/GaAs Quantum Dots, Academic Press, 60, 1999.